5.3 Comparison of wavelet and eddy-covariance techniques for computation of fluxes in intermittent turbulence over a mountain basin

Sandra J. Cardon[1*], Robert D. Kelly[1], David C. Leon[1], Dean Vickers[2], Larry Mahrt[2]
[1]University of Wyoming, Laramie, Wyoming
[2]Oregon State University, Corvallis, Oregon

1. Introduction

The field phase of the Fluxes Over Snow Surfaces (FLOSS) project occurred in February and March 2003, in the North Park mountain basin in northern Colorado. The average elevation at the field site is approximately 2450 m. The basin is roughly rectangular in shape and is bounded by mountains extending to 3600 m in elevation on the eastern and western sides, with lower ridges on the northern and southern ends of the basin.

Research platforms employed during FLOSS included a 30-m surface layer tower (the ISFF tower, NCAR), three 2-m towers located in areas of different vegetation types, and the University of Wyoming King Air research aircraft. Both the tower and the aircraft included fast-response instruments for eddy covariance computation of sensible heat, moisture, and momentum fluxes. Slow response instruments were available for determining state variables including temperature, water vapor mixing ratio, pressure, and wind speed and direction. Fluxes from the ISFF tower during FLOSS have been examined in the context of assessing the effect of vegetation on sublimation and melting of snow, Mahrt and Vickers (2005).

Most of the aircraft data were collected in repeated, low-level legs about 12 km long at 60 m above ground level (AGL) passing near the tower. This pattern was interrupted about every six passes for an aircraft sounding to well above the inversion layer. The aircraft flight track A-A, shown in Figure 1, was oriented southeast to northwest, parallel to two ridges, the Peterson Ridge and the Owl Ridge, that were about 2 km southwest of the track and tower.

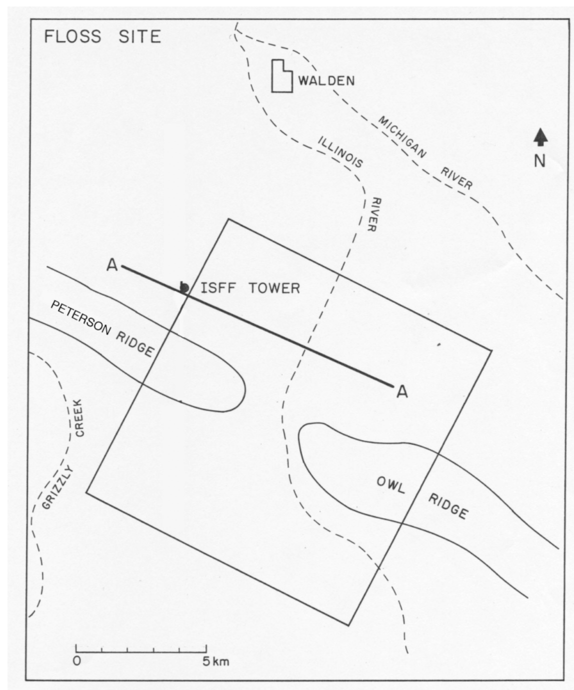

Figure 1. Map of the FLOSS experiment area showing the ISFF tower and the primary aircraft flight line (A-A).

Vegetative cover along the flight track consisted primarily of patches of short prairie grass, sagebrush, and other brush, with hay meadows and willows occupying the area along the Illinois River, which flows south to north though a gap between the two ridges. The terrain along the flight track was highest at the southeast end, atop the Illinois escarpment, sloping down to the stream, and was nearly level west of the stream to the northwest end of the flight track. A picture from one of the cases examined here is shown in Figure 2.

*Corresponding author address: Sandra J. Cardon, Atmospheric Science Department, University of Wyoming, Laramie, WY 82071; email: sandyj@uwyo.edu

Figure 2. View southeast across North Park from the King Air on February 18, 2003. ISFF tower is barely visible in the middle-left of the image. R. Kelly photo.

The aircraft data are of interest because the on-site times – most starting before dawn with two flights later in the afternoon -- were usually those of noticeable heterogeneity in the upper surface layer (SL) and boundary layer (BL). On most of the flight legs, the time series for the eddy flux variables were visibly non-stationary, and thus not amenable to the computation of single covariance values for complete legs.

Sources of heterogeneity along the flight track included changes in dynamic and static stability, including the night-to-day transition; variations in the depth and extent of the snow cover leading to changes in surface albedo, energy balance, and temperature; variations in the height of the vegetation relative to the snow depth, with some portion of the vegetation usually extending above the snow surface; changes in vegetation type resulting in varying color and radiation absorption; variations in terrain, including the ridges just southwest of the tower and flight track, which are interrupted by the Illinois River, flat bottom-land along the river, and a sharp rise in elevation just east of the stream; mesoscale currents in the mountain basin; and variations in cloud cover both with distance along the flight track and with time during any given flight.

This paper presents several different techniques for calculating eddy fluxes in a heterogeneous environment, primarily based on **(1)** simple covariances for short segments of each flight track, and **(2)** integration of the two-dimensional cospectra from wavelet analyses of the same tracks. The wavelet analyses utilize the non-orthogonal Morlet wavelet, as applied in the subroutine supplied by Torrence and Compo (1998). The Morlet wavelet is a complex sinusoid modulated by a Gaussian, and was chosen by the authors to be suitable for SL and BL turbulence. Empirical correction factors supplied by Torrence and Compo (1998, Table 2) were used in the integration of the wavelet cospectra, and are needed to compensate for the non-orthogonality of the Morlet functions.

2. Instrumentation

Eddy flux instruments onboard the UW King Air included a Rosemount 858 three-dimensional gust probe, with wind measurement converted to be ground-relative using data from an inertial reference system and a GPS receiver. Fast-response temperatures were measured with an in-house designed and constructed reverse-flow probe. Fast-response water vapor mixing ratio was measured with a Lyman-alpha wavelength absorption device from NCAR. Offsets in the Lyman-alpha mixing ratios were removed using low-rate data from an EG&G chilled-mirror hygrometer.

Cloud conditions for the flights were assessed using the downwelling IR radiation in addition to photographs and video recordings from the cockpit.

King Air data used for the flux calculations were output at 50 Hz resulting in a Nyquist frequency of 25 Hz. The average airspeed of the King Air is ~85 m s^{-1} so a single point corresponds to just under 2 m and each 12 km leg consists of just over 7000 points.

3. Cases

Two different cases are considered here: February 18 and March 21, 2003. The February 18 flight took place early in the morning with data collection beginning before dawn. Along the flight track, between the tower and the river bottom and on the escarpment at the southeast end of the leg was almost completely snow covered. The rest of the flight track had only scattered snow cover. During the flight, the winds were calm (~2 m s^{-1}). The flight interval captured the transition between the stable, nighttime BL and the unstable, daytime BL.

In contrast, the March 21 flight took place in the mid- to late-afternoon under convectively unstable BL conditions. There was little to no snow cover northwest of the tower. Between the tower and the river there was more snow cover, while atop the escarpment the snow cover was almost complete. The winds during the flight were relatively strong (~7 m s^{-1}).

Figure 3 shows the time traces for w and T' from a single leg from each flight. The traces from February 18 are visibly heterogeneous with intermittent turbulent and quiescent periods. In contrast, the traces from March 21 are apparently homogeneous. The contrast between these two cases affords us an opportunity to examine how different approaches to computing the eddy covariance fluxes behave under different conditions.

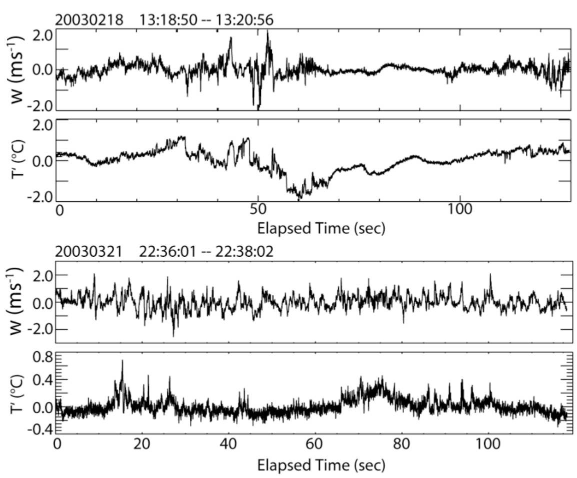

Figure 3. Time series of aircraft-measured vertical velocity (w) and temperature perturbation (T') for flight legs from February 18 and March 21, 2003.

4. Flux Calculations

The continuous wavelet transformation was applied to the time series of vertical air velocity, temperature, water vapor, and horizontal winds. Combining the continuous wavelet transformation of two time series gives the wavelet cospectra, which is a function of both time (or position) and frequency. The wavelet cospectra are useful for visualizing which locations/frequencies contribute significantly to the covariance (or flux) between the series, but are difficult to use quantitatively. By integrating the wavelet cospectra over a range of frequencies (using the empirical correction factor), an estimate of the covariance as a function of time/location was obtained. In this paper, the wavelet cospectra were integrated from 0.1 Hz up to the Nyquist limit of 25 Hz. We refer to the resulting time-series as the 'integrated cospectra'. An example of the w' and T' series, wavelet cospectra, and the resulting integrated cospectra for a single leg on February 18 are shown in Figure 4.

The width of the Gaussian envelope that modulates the sinusoidal oscillations increases with decreasing frequency. At the 0.1 Hz lower limit used for the integration, the width of the Gaussian envelope where it drops to 5% of the maximum value encompasses 2000 points, or 40 s (~3.5 km) of data. At 0.1 Hz, only a third of the data points in the wavelet spectra/cospectra are influenced by the ends of the leg. This fraction increases for lower frequencies, and by 0.03 Hz the entire series is within the influence of the ends of the leg.

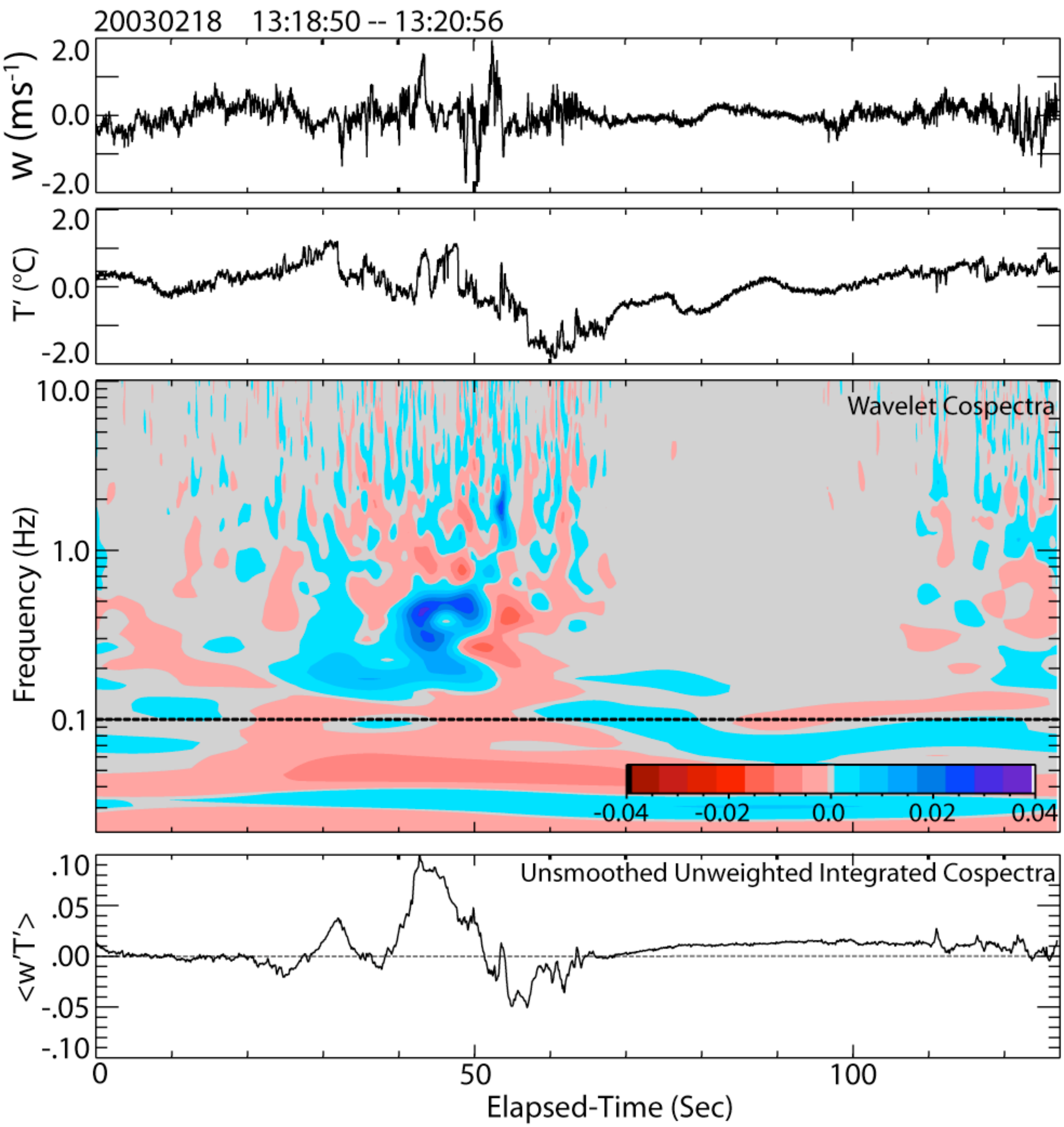

Figure 4. Time series of w and T′ for a single, ~10 km flight leg, the corresponding wavelet cospectra, and (unsmoothed, unweighted) integrated cospectra obtained by integrating the wavelet cospectra for frequencies above 0.1 Hz (indicated by the dashed line). The two series are clearly highly non-stationary with most of the variance and covariance originating within a single 40 s interval.

The covariance was also calculated directly over 100-m segments, thus covering frequencies from 1 to 25 Hz (where the airspeed of the King Air has been approximated as 100 m s^{-1} for convenience). The covariance calculated for individual 100-m segments produces a noisier output because each 100-m segment consists of only ~50 points. In contrast, the integrated cospectra encompasses up to 2000 points (at the 0.1 Hz lower integration limit). Further smoothing the covariance using a running average over 5 and 19 segments, each 100 m in length (for a total length of 0.5 km and 1.9 km, respectively), covers a range of about 6 and 22 s and a total of 250 and 950 data points respectively, using the actual average true air speed of 85 m s^{-1}.

In order to compare the integrated cospectra with the covariance calculated using a 100-m window, the integrated cospectra were first averaged over 100-m segments, effectively reducing the integrated cospectra to a 1 Hz output. These averages were in turn averaged over 5 and 19 segments, thus covering the same time and distances as used for the covariances. Even before smoothing, the integrated cospectra were less noisy than the covariances because of the effects of the wavelet convolutions – an effect furthered by the additional smoothing over 5 and 19 100-m segments. Since the turbulence can be highly non-uniform, edge effects can drastically skew the output if areas of high and low turbulence are averaged together. In order to reduce this effect, the integrated cospectra were also averaged over 5 and 19 segments using center-weighted averaging thus decreasing the effects of the end-most points for each average.

The covariance and integrated cospectra were plotted via two methods. First, they were plotted for each flight leg with respect to time as shown in Figure 4. Then, all passes for a given day were combined, and the fluxes for an entire flight were plotted with respect to both time and distance along the flight track as shown in Figure 5. The position of the aircraft was projected into distance along the flight track to allow for consistency between flight-legs and different flights in order to help assess the effect of varying terrain, vegetation and snow cover. After all plotting was complete, there were eight separate cases: **(1)** 100 m covariance; **(2)** unsmoothed, unweighted integrated cospectra; **(3)** 100 m, 5 segments per window smoothed unweighted covariance, **(4)** unweighted and **(5)** center-weighted averaged integrated cospectra; **(6)** 100 m, 19 segments per window smoothed unweighted covariance, **(7)** unweighted and **(8)** center-weighted averaged integrated cospectra.

5. Flux Comparisons

One main objective was to determine the "best" method of the above mentioned eight. When comparing the covariance with the integrated cospectra, several factors arose. The 100-m covariance was initially unsmoothed while the integrated cospectra imply some smoothing due to the frequency-varying convolutions as previously mentioned. The 100-m covariance covered a frequency range of 1-25 Hz, while the integrated cospectra covered 0.1-25 Hz. Since the main flux events occurred between 1 Hz and 0.1 Hz, or roughly 100 m and 1 km, the covariance calculations missed the main flux events while the integrated cospectra captured them. Thus, the two methods were a compromise. If the calculated covariance was taken over too large of an interval, then intermittence and heterogeneity interfered. Adjacent areas of negative and positive fluxes lead to some or all of the net flux being zero; the values for narrow areas of strong fluxes may be drastically reduced.

Figure 5 shows the magnitude of temperature flux difference between the integrated cospectra February 18, 2003 and March 21, 2003 flights with respect to time and distance along the flight track.

The fluxes on February 18 are mainly negative, while on March 21, they are predominately positive due to the surface heating in the convectively stable BL. The surface heating leads to positive temperature fluxes and positive moisture fluxes due to sublimation and melting/evaporation of the snowpack.

The smoothing interval also changes the fluxes significantly, as shown in Figure 5. The smoothing over 0.5 km (5 segments) preserved most of the unsmoothed magnitude and features along with the shape of the time series, but was still very noisy. Averaging over 1.9 km still preserved the major features, while eliminating the minor features and drastically reducing the magnitude of the unsmoothed series. This is expected since the flux sign can change instantaneously and the 1.9 km averaging smoothes over more areas with both positive and negative fluxes, thus driving the average resulting flux closer to zero. The center-weighted averaging reduces the effects of smoothing by weighting the center-most points of the window the most, and thus best preserves the original shape and magnitude. The exact percentages of preserved magnitude through various smoothing and averaging techniques vary drastically between variables, flights, and individual flight legs.

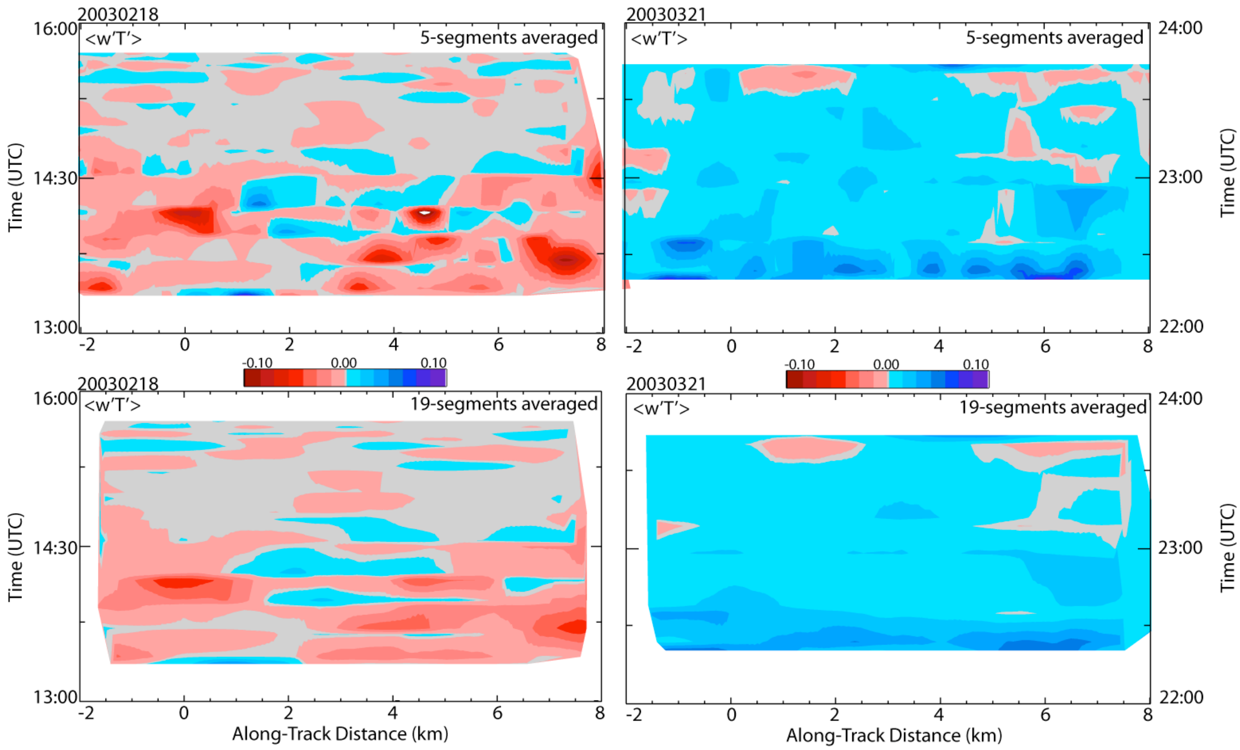

Figure 5. Contour plots smoothed over 5 and 19 100-m segments for February 18, 2003 and March 21, 2003

Plotting histograms of the fluxes allows the smoothing trends shown in the contour plots to be quantified. Comparing the 0.5 km and 1.9 km smoothing, the unweighted covariance, and the unweighted and center-weighted integrated cospectra shown in Figure 6, one can see that for the 19-segment averaging, the frequency distribution is narrower. It is also natural that in the unsmoothed cases of covariance and integrated cospectra, the integrated cospectra would have a narrower frequency distribution due to the frequency dependent convolutions.

For the case of February 18, 2003, as the day progresses, the turbulence becomes more uniform compared to earlier in the day which leads to a narrower frequency distribution.

For the case of March 21, the frequency distribution is narrow, due to the relatively homogeneous turbulence profile, and offset slightly from zero corresponding to a positive heat flux.

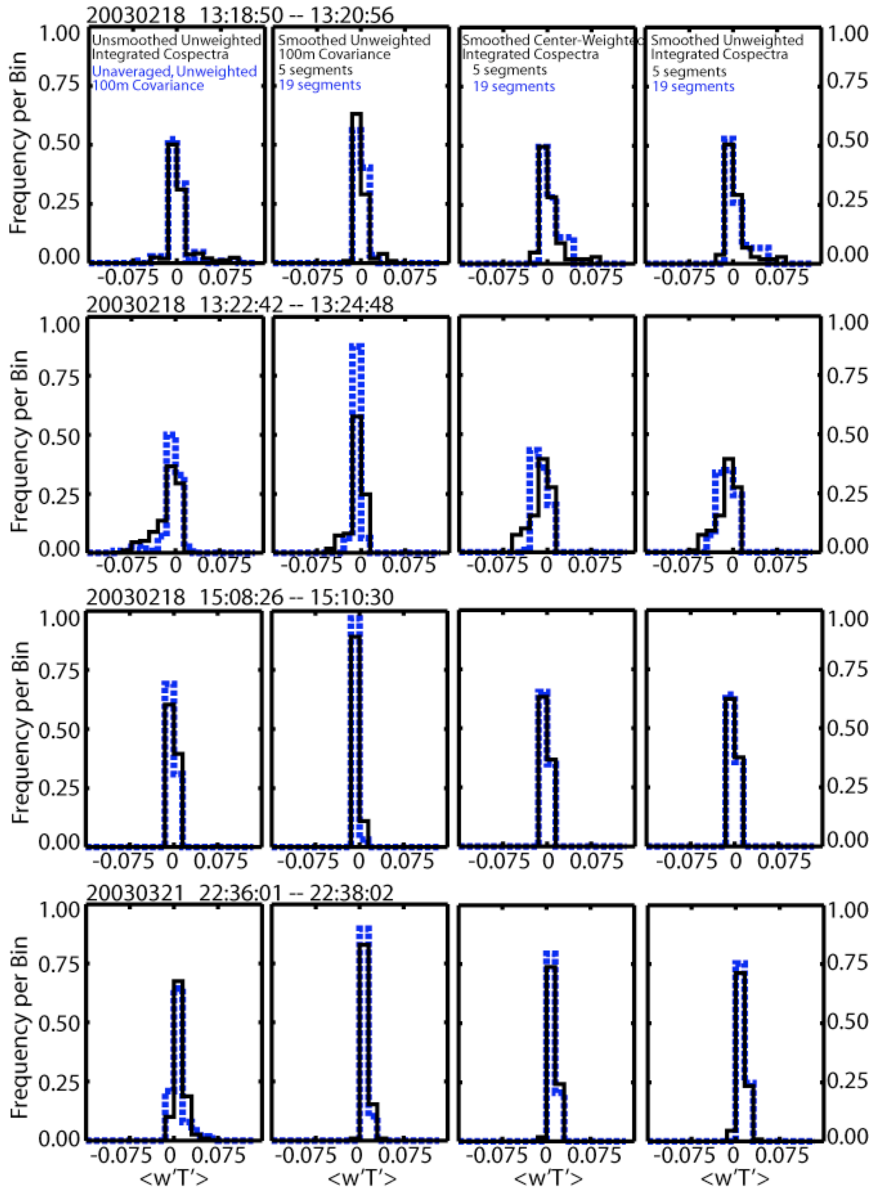

Figure 6. Histograms of the w-T covariance and integrated cospectra for four example flight legs values using the approaches discussed in Section 4.

6. Conclusions

The authors are not aware of an objective test to determine which of the flux methods is best. However, wavelet decomposition is designed to detect spectral variability in the two-dimensional space of time and frequency, so wavelet cospectra seem well-suited to the task. It appears that the integrated wavelet cospectra are best at estimating the eddy fluxes in a heterogeneous, intermittent environment.

Both the integrated cospectra and the 100-m covariance, as applied here, raise issues of scale. The integration has been truncated at 0.1 Hz, i.e., at a scale of about 1 km. Our justifications for applying this cutoff to the integration of the wavelet cospectra are: **(1)** the BL is much shallower than 1 km, so the upper limit on isotropic eddy size is less than 1 km, **(2)** while larger eddies are probably present, they are very difficult to detect and measure in this heterogeneous environment, **(3)** both the tower and the aircraft flight track are about 2 km from the most prominent terrain feature in the area, namely the ridge to the southwest of both, **(4)** for frequencies lower than 0.1 Hz, the cone of influence of the ends of the series encompasses most of the series. The 100-m segment for covariance limits the eddy scales to 100 m and smaller, i.e., about 0.1 Hz and higher. Thus, there is a size range (0.1-1 Hz, or about 100 m to 1 km) that is detected by the integrated cospectral fluxes, but not by the covariance fluxes. Making the covariance segments much longer than 100 m allows the flux contributions from heterogeneous regions to be detected, but casts doubt on the resulting fluxes due to the non-stationarity of the series.

Averaging subsequent to the calculation of the 100-m covariance or integrated cospectra amounts to different smoothing of the flux estimates. The best duplication of the integrated cospectra, for both magnitude and shape, is obtained using the center-weighted averaging that was applied over 500 m. This covers five 100-m segments, and reduces the influence of heterogeneous changes at the end points of the 500-m periods. The segment length of 100 m and the averaging length of 500 m are somewhat arbitrary choices, but they seem effective for these cases.

Averaging the 100-m segments over 1.9 km using either simple averages or center-weighted averages seems too long an interval for this situation and fails to capture most of the fluxes.

7. References

Mahrt, L. and D. Vickers, 2005: Moisture fluxes over snow with and without protruding vegetation. *Quart. J. Roy. Meteor. Soc.*, **131**, 1251-1270.

Torrence, C. and G. P. Compo, 1998: A practical guide to wavelet analysis. *Bull. Amer. Meteor. Soc.*, **79,** 61-78.